Galactose oxidase models: insights from ^{19}F NMR spectroscopy†

Fabien Michel,[a] Sylvain Hamman,[a] Christian Philouze,[a] Carlos Perez Del Valle,[b] Eric Saint-Aman[a] and Fabrice Thomas*[a]

Received 29th July 2008, Accepted 2nd October 2008
First published as an Advance Article on the web 28th November 2008
DOI: 10.1039/b813036a

^{19}F labelled tripodal ligands that possess a N_3O donor set (one phenol, one tertiary amine and either two pyridines or one pyridine and one quinoline) have been synthesized. The fluorine is incorporated either at the phenol O-donor (HL^F and HL^{CF3}) or at the quinoline N-donor (HLq^{OMe} and HLq^{NO2}). The copper(II)–phenol complexes $(2H)^{2+}$, $(1H)^{2+}$, $(3H)^{2+}$ and $(4H)^{2+}$ as well as the corresponding copper(II)–phenolate complexes have been characterized. X-Ray diffraction reveals an increase in the oxygen–copper bond distance of more than 0.4 Å upon protonation of the phenolate moiety of $(4)^+$. Protonation is accompanied by an axial to equatorial isomerization of the quinoline group. DFT calculations show that stretching of the Cu–O(phenol) bond, π-stacking interactions and rotation of the pyridine are key steps in this isomerization process. Protonation, and thus changes in the oxygen–copper bond distance induce either a decrease ($(1H)^{2+}$, $(2H)^{2+}$) or an increase ($(3H)^{2+}$ and $(4H)^{2+}$) in the copper–fluorine distance that could be monitored by ^{19}F NMR. In the former case, a broadening of the ^{19}F NMR signal is observed, whereas a sharpening is observed in the latter case. Temperature dependent ^{19}F NMR measurements on equimolar mixtures of the phenol and phenolate complexes of $(3)^+$ and $(4)^+$ reveal rate constants for proton transfer and/or isomerization of 3000 ± 100 s^{-1} and 2900 ± 100 s^{-1}, respectively, at the coalescence temperature. This temperature was found to be strongly affected by the phenol *para*-substituent as it is 226 K and *ca.* 330 K for $(3)^+$ and $(4)^+$, respectively. A phenoxyl radical species ($(3^{\bullet})^{2+}$) could be generated and characterized for the first time by ^{19}F NMR spectroscopy.

Introduction

Galactose oxidase (GO) is a copper(II) enzyme that catalyses the oxidation of primary alcohols into the corresponding aldehydes, with concomitant reduction of dioxygen into hydrogen peroxide.[1] The crystal structure of GO was reported in 1991, showing an active site constituted by a copper ion in a square pyramidal geometry.[2] It is coordinated in the basal plane to two histidine nitrogen atoms (His_{496}), one tyrosinate oxygen (Tyr_{272} that is cross-linked with Cys_{228}), and one exogenous ligand (acetate molecule from the buffer). The apical position is occupied by one tyrosine oxygen (Tyr_{495}). The apparent paradox—a two-electron oxidation performed by a single copper ion—is explained by the involvement of another redox center, namely a tyrosyl radical from the protein, during the catalytic cycle. Extensive characterizations have shown that it is located at $Tyr_{272}^{\bullet}$ and that it is essential for catalysis.[1]

Several model compounds for the GO active site have been developed during the last decade, contributing to an enhanced understanding of the metal–radical interaction.[3–10] In this context, it has been shown that tripodal ligands were good structural, and sometimes functional, models of GO.[3–10] In particular, the copper complex of HL^{OMe} (Fig. 1) has been shown to be a structural model that reproduces quite well the spectroscopic properties and reactivity of the enzyme.[6]

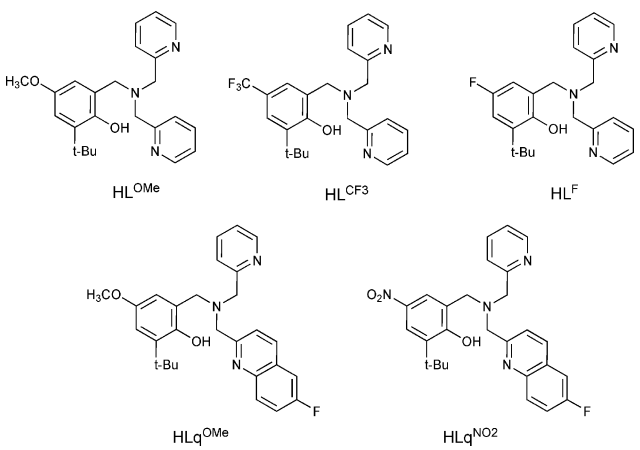

Fig. 1 Formulae of the tripodal ligands.

Techniques that are commonly used in order to characterize such complexes are UV-vis and EPR spectroscopies, as well as electrochemical measurements. The development of new tools to study GO models is of major interest. For example, classical techniques do not enable the discrimination in the phenol(ate) position (axial *vs.* equatorial), and dynamic information is generally missing. We have recently shown that ^{19}F NMR could be a very powerful tool when it is combined with judicious ligand labelling.[7] This technique offers unique advantages as a lack of

[a]*Département de Chimie Moléculaire, Chimie Inorganique Redox Biomimétique (CIRE), UMR CNRS 5250, Université J. Fourier, B. P. 53, 38041 Grenoble cedex 9, France. E-mail: Fabrice.Thomas@ujf-grenoble.fr; Fax: +33 476 514 846; Tel: +33 476 514 373*
[b]*Département de Chimie Moléculaire, Chimie Théorique, UMR CNRS 5250, Université J. Fourier, B. P. 53, 38041 Grenoble cedex 9, France*

† Electronic supplementary information (ESI) available: Additional EPR, CV and titration curves. CCDC reference numbers 661385 and 661386. For ESI and crystallographic data in CIF or other electronic format see DOI: 10.1039/b813036a

interfering background signals, high sensitivity and distribution of resonances over a wide spectral width. HLq^{NO2} (Fig. 1) is derived from HL^{OMe}: The fluorine atom has been incorporated in the ligand by replacing the pyridine by a fluoroquinoline group, while the methoxy substituent was replaced by a nitro one (in order to monitor proton transfers and not radical formation).[7] In its copper(II) complexes, we have shown that both the chemical shift and the line width of the ^{19}F resonance are extremely sensitive to protonation and phenol positioning.

Is it possible to extrapolate these results to other systems? We here address this question through the study of a series of ^{19}F-labelled ligands derived from HL^{OMe}. More specifically, we explore (i) different kinds of ligand labelling and, as this work deals with the modelling of the GO active site, (ii) the possibility to directly detect phenoxyl radicals by ^{19}F NMR.

The ligand HLq^{OMe} (Fig. 1) differs from HLq^{NO2} by its phenol *para*-substituent, a strongly electron-donating methoxy group. This substituent is known to stabilize phenoxyl radicals very efficiently.[3–6] HLq^{OMe} is thus expected to be the precursor of stable phenoxyl radicals, as does HL^{OMe}.

HL^{CF3} and HL^{F} belong to another family of F-labelled tripodal ligands in which the fluorine atom is introduced on the phenol moiety and not on a N-donor (Fig. 1). The ligands differ to each other by the phenolate *para*-substituent, a trifluoromethyl group in HL^{CF3} or a fluorine atom in HL^{F}.

Synthesis of these ligands and their copper(II) complexes is described, as well as their characterization by electrochemical and spectroscopic methods (including ^{19}F NMR).

Results and discussion

Preparation of the ligands

HL^{CF3} was obtained in a one-pot synthesis by mixing bis(2-pyridylmethyl)amine and 2-*tert*-butyl-4-trifluoromethanephenol in the presence of one equivalent of formaldehyde. HLq^{OMe} was prepared in a similar way to HLq^{NO2} by using 3-*tert*-butyl-2-hydroxy-5-methoxybenzaldehyde. HL^{F} and HLq^{NO2} have been previously described.[6–7]

Crystal structures of the copper complexes

Monomeric complexes were obtained upon mixing stoichiometric amounts of the N_3O ligands and $Cu(ClO_4)_2\cdot 6H_2O$ in acetonitrile. Under these conditions, the complexes were isolated in their protonated form in which the phenolic subunit remains protonated. Single crystals of $[Cu^{II}(HL^{CF3})(CH_3CN)]^{2+}$ $(1H)^{2+}$, $[Cu^{II}(HL^{F})(CH_3CN)]^{2+}$ $(2H)^{2+}$,[6] $[Cu^{II}(HLq^{OMe})(CH_3CN)]^{2+}$ $(3H)^{2+}$ and $[Cu^{II}(HLq^{NO2})(CH_3CN)]^{2+}$ $(4H)^{2+}$[7] were obtained upon slow diffusion of di-*iso*-propyl ether into acetonitrile solutions of the complexes (Table 1). When one equivalent of $Cu(ClO_4)_2\cdot 6H_2O$ and HLq^{NO2} were mixed in acetonitrile in the presence of NEt_3, the phenolate copper complex $(4)^+$ could be crystallized.[7] The ORTEP plots of these complexes are depicted in Fig. 2 and selected bond lengths and angles are listed in Table 2.

In $(1H)^{2+}$ and $(2H)^{2+}$, the geometry around the metal center is octahedral with one phenol oxygen and one perchlorate oxygen atom that coordinate in axial positions. An exogenous acetonitrile, two pyridines and the tertiary amine nitrogen atoms occupy the equatorial positions.

Table 1 Crystal data for $(1H)^{2+}$ and $(3H)^{2+}$

	$(1H)(ClO_4)_2$	$(3H)_2(ClO_4)_4\cdot CH_3CN$
Formula	$C_{26}H_{29}Cl_2CuF_3N_4O_9$	$C_{62}H_{69}Cl_4Cu_2F_2N_9O_{20}$
M_r/g mol^{-1}	732.98	1567.18
Crystal system	Monoclinic	Triclinic
Space group	$P2_1/c$	$P\bar{1}$
a/Å	8.672(3)	12.006(3)
b/Å	40.05(2)	17.558(4)
c/Å	8.855(5)	18.513(2)
α/°	90	67.13(1)
β/°	101.2(1)	73.91(1)
γ/°	90	82.21(2)
V/Å^3	3017(3)	3453(1)
Z	4	2
T/K	150	150
D_c/g cm^{-3}	1.614	1.507
μ/cm^{-1}	9.78	8.55
Monochromator	Graphite	Graphite
λ/nm	MoKα (0.71073 Å)	MoKα (0.71073 Å)
Reflections collected	29 657	26 103
Independent reflections	7549	9241
Observed reflections	4419 [$I > 2\sigma(I)$]	6328 [$I > 2\sigma(I)$]
R_{int}	0.1255	0.1088
R_1	0.0436	0.0719
wR_2	0.0396	0.0972

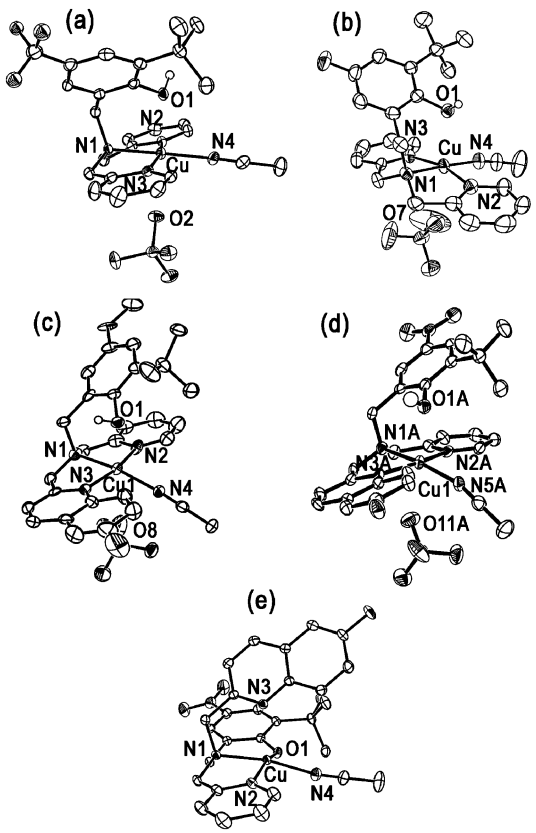

Fig. 2 ORTEP plot of: (a) $(1H)^{2+}$ (ClO_4^-); (b) $(2H)^{2+}$ (ClO_4^-);[6] (c) $(3H)^{2+}$ (ClO_4^-); (d) $(4H)^{2+}$ (ClO_4^-)[7] and (e) $(4)^+$.[7] Ellipsoids are drawn at the 50% probability level and hydrogen atoms (except the phenolic ones) are omitted for clarity.

Table 2 Selected bond distances (Å) and angles (°)

$(1H)\cdot 2ClO_4$					
Cu–O1	2.353(2)	Cu–O2	2.526(2)	Cu–N1	2.026(2)
Cu–N2	1.992(2)	Cu–N3	1.980(2)	Cu–N4	1.988(2)
N1–Cu–N2	83.0(1)	N1–Cu–N3	84.3(1)	N1–Cu–N4	176.3(1)
N2–Cu–N3	165.5(1)	N2–Cu–N4	93.9(1)	N3–Cu–N4	98.6(1)
$(2H)\cdot 2ClO_4$					
Cu–O1	2.404(3)	Cu–N1	2.024(4)	Cu–N2	1.976(4)
Cu–N3	1.975(3)	Cu–N4	2.008(4)	Cu–O7	2.600(4)
N1–Cu–N2	83.7(2)	N1–Cu–N3	84.0(1)	N1–Cu–N4	177.4(2)
N2–Cu–N3	163.6(1)	N2–Cu–N4	95.0(2)	N3–Cu–N4	96.9(2)
$(3H)\cdot 2ClO_4$					
Cu1–O1	2.415(5)	Cu1–O8	2.631(5)	Cu1–N1	2.014(4)
Cu1–N2	1.981(4)	Cu1–N3	2.016(4)	Cu1–N4	1.980(5)
N1–Cu1–N2	83.8(2)	N1–Cu1–N3	82.8(2)	N1–Cu1–N4	166.2(2)
N2–Cu1–N3	165.9(2)	N2–Cu1–N4	92.0(2)	N3–Cu1–N4	100.0(2)
Cu2–O3	2.355(4)	Cu2–O17	2.631(5)	Cu2–N5	2.005(5)
Cu2–N6	2.002(4)	Cu2–N7	2.010(4)	Cu2–N8	1.978(5)
N5–Cu2–N6	83.7(2)	N5–Cu2–N7	82.2(2)	N5–Cu2–N8	164.7(2)
N6–Cu2–N7	165.7(2)	N6–Cu2–N8	90.6(2)	N7–Cu2–N8	102.5(2)
$(4H)\cdot 2ClO_4$					
Cu1–O1A	2.363(3)	Cu1–O11A	2.615(4)	Cu1–N1A	2.008(4)
Cu1–N2A	2.002(4)	Cu1–N3A	2.038(4)	Cu1–N5A	1.996(4)
N2A–Cu1–N1A	83.86(16)	N1A–Cu1–N3A	82.24(16)	N5A–Cu1–N1A	169.83(17)
N2A–Cu1–N3A	165.20(14)	N5A–Cu1–N2A	91.85(16)	N5A–Cu1–N3A	101.03(16)
Cu2–O1B	2.637(4)	Cu2–O21B	2.650(4)	Cu2–N1B	1.994(3)
Cu2–N2B	1.976(4)	Cu2–N3B	1.985(4)	Cu2–N5B	1.972(4)
N2B–Cu2–N1B	84.67(15)	N3B–Cu2–N1B	81.90(14)	N5B–Cu2–N1B	166.45(17)
N2B–Cu2–N3B	166.55(14)	N5B–Cu2–N2B	93.79(17)	N5B–Cu2–N3B	99.46(16)
$(4)\cdot ClO_4$					
Cu–O1	1.905(1)	Cu–N1	2.053(1)	Cu–N2	1.965(1)
Cu–N3	2.229(1)	Cu–N4	2.015(2)	O1–Cu–N1	94.27(5)
O1–Cu–N2	161.74(5)	O1–Cu–N3	93.18(5)	O1–Cu–N4	83.78(6)
N1–Cu–N2	83.53(6)	N1–Cu–N3	82.62(5)	N1–Cu–N4	168.67(5)
N2–Cu–N3	104.46(5)	N2–Cu–N4	94.82(6)	N3–Cu–N4	108.60(5)

For $(1H)^{2+}$, the $Cu–N_{tertiary\ amine}$ bond distance Cu–N1 is 2.026(2) Å, while the $Cu–N_{pyridine}$ bond distances Cu–N2 and Cu–N3 are 1.992(2) and 1.980(2) Å, respectively. They are within the range of those reported for $(2H)^{2+}$ (2.008(4), 1.976(4) Å and 1.975(3) Å for Cu–N1, Cu–N2 and Cu–N3, respectively)[6] and some other related complexes.[3–10]

The $Cu–O_{phenol}$ bond distances are 2.353(2) and 2.404(3) Å for $(1H)^{2+}$ and $(2H)^{2+}$, respectively. These values are much higher than those reported for axial $Cu–O_{phenolate}$ bonds (typically around 2.2 Å),[7–10] thus showing that the phenolic unit remains only weakly coordinated to the metal center. In both complexes, the $Cu–O_{perchlorate}$ bond distance is much longer (2.526(2) and 2.600(4) Å for $(1H)^{2+}$ and $(2H)^{2+}$, respectively), in agreement with an even weaker $Cu–O_{perchlorate}$ bond. The phenol unit is found to be π-stacked over one pyridine ring with a distance between the two centroids of 4.04 and 4.09 Å for $(1H)^{2+}$ and $(2H)^{2+}$, respectively.

In both $(3H)^{2+}$ and $(4H)^{2+}$, the crystal cell contains two independent complexes. The geometry around the metal center is close to that observed in $(1H)^{2+}$ and $(2H)^{2+}$, *i.e.* octahedral with the axial positions occupied by one phenol oxygen and one perchlorate oxygen atom. The equatorial positions are occupied by nitrogen atoms from an exogenous acetonitrile, the pyridine, the quinoline and the tertiary amine.

In the two independent complexes present in the crystal cell of $(3H)^{2+}$ the $Cu–N_{pyridine}$ bond distances Cu1–N2 and Cu2–N6 are 1.981(4) and 2.002(4) Å, the $Cu–N_{quinoline}$ bond distances Cu1–N3 and Cu2–N7 are 2.016(4) and 2.010(4) Å, while the $Cu–N_{tertiary}$ amine bond distances Cu1–N1 and Cu2–N5 are 2.014(4) and 2.005(5) Å. The corresponding bond distances in the previously described complex $(4H)^{2+}$ were found to be roughly similar, with Cu1–N2A = 2.002(4) Å and Cu2–N2B = 1.976(4) Å for the $Cu–N_{pyridine}$ bonds, Cu1–N3A = 2.038(4) Å and Cu2–N3B = 1.985(4) Å for the $Cu–N_{quinoline}$ bonds, and Cu1–N1A 2.008(4) Å and Cu2–N1B 1.993(3) Å for the $Cu–N_{tertiary}$ amine bonds.[7] The increase in bond length observed for the $Cu–N_{quinoline}$ bond compared to the $Cu–N_{pyridine}$ one is ascribed to steric hindrances around the nitrogen atom of the quinoline that consequently weakens the Cu–N bond. Similar increases in bond lengths have been reported in copper(II) complexes of tripodal ligands when pyridines are α-methylated.[9] The $Cu–O_{phenol}$ bond distances in $(3H)^{2+}$ are Cu1–O1 = 2.415(5) Å and Cu2–O3 = 2.355(4) Å, whereas the $Cu–O_{perchlorate}$ bond lengths Cu1–O8 and Cu2–O17 are longer (2.631(5) Å and 2.631(5) Å,

respectively). This trend is similar to that observed in $(1H)^{2+}$, $(2H)^{2+}$ and $(4H)^{2+}$. As in these latter complexes, the phenol is π-stacked over the pyridine ring at a distance of 3.85 and 3.99 Å (between the two centroids).

In $(4)^+$, the geometry was found to be quite different:[7] the copper(II) ion resides within a square pyramidal geometry. The quinoline nitrogen binds in the axial position, while the phenolate moiety, an exogenous acetonitrile, the pyridine and the tertiary amine nitrogen atoms occupy the equatorial positions. The Cu–$O_{phenolate}$ bond is stronger than in $(4H)^{2+}$ as reflected by a shorter Cu–O bond distance (1.905(1) Å). In addition, it is the phenolate and the quinoline rings that are involved in intramolecular π-stacking interactions (and not the phenol with one pyridine unit).

In the Cu^{II}-phenol complexes $(1H)^{2+}$, $(2H)^{2+}$, $(3H)^{2+}$ and $(4H)^{2+}$, the Cu···OH(Ar) bond is weak and consequently the phenol systematically occupies the more labile, *i.e.* axial, position. Weak interactions between the copper ion and one perchlorate molecule (as a sixth ligand) could also be detected at the solid state. In the Cu^{II}-phenolate complex $(4)^+$, the Cu···O^-(Ar) bond is stronger, as reflected by the shorter Cu–O bond distance, and no more interaction with the perchlorate anion exists. Some X-ray crystal structures of Cu^{II}-phenolate complexes built from N_3O ligands derived from the bis(pyridylmethyl)amine or bis(pyridylethyl)amine have been reported.[7–9] In the bis(pyridylmethyl)amine derivatives, the phenolate occupies the axial position, except when one (or both) pyridine(s) is(are) α-methylated;[9] in this particular case, the X-ray crystal structure analysis reveals an equatorial positioning of the phenolate. Steric hindrances around the quinoline nitrogen of $(4)^+$ (as in α-methylpyridines), as well as the π-stacking interactions between the phenolate and quinoline rings (see below) may contribute to the isomerization.

Spectroscopic and electrochemical properties of the copper complexes

The UV-vis spectra of the phenol complexes $(1H)^{2+}$, $(2H)^{2+}$, $(3H)^{2+}$ and $(4H)^{2+}$ in CH_3CN are characterized by copper(II) d–d transitions at around 600 nm, in agreement with a square planar, or elongated octahedral geometry, around the metal. The addition of NEt_3 to these complexes results in the appearance of a phenolate-to-copper CT transition as expected for deprotonation of the phenolic moiety.[6] The so-obtained deprotonated species $(1)^+$, $(2)^+$, $(3)^+$ and $(4)^+$ exhibit a CT transition at 500, 535, 560 and 510 nm, respectively (Fig. 3, Table 3). In each sub-series (ligands bearing either two pyridines or one pyridine and one quinoline), the λ_{max} is shifted according to the electronic properties of the phenolate substituent, with the highest λ_{max} observed for the electron-donating methoxyl group and the lowest for the electron-withdrawing nitro and trifluoromethyl groups.[6] In their EPR spectra all the complexes exhibit a ($S = 1/2$) signal with copper(II) hyperfine structure, indicating that the mononuclear structures are preserved in CH_3CN (Fig. 4).

The phenolate complexes $(1)^+$, $(2)^+$, $(3)^+$ and $(4)^+$ exhibit in their CV curves a one-electron oxidation wave centered at $E_{1/2}$ = 0.56, 0.20, 0.09 and 0.83 V *vs.* Fc/Fc^+, respectively. These values correlate with the σ^+ Hammet of the phenolate *para*-substituent, suggesting that the ligand is involved in the oxidation process. In addition, the value of 0.09 V for $(3)^+$ is close to those reported for the oxidation of copper(II) coordinated methoxyphenolates into methoxyphenoxyl radicals,[6,12] further confirming that the redox process corresponds to the oxidation of the phenolate into a phenoxyl radical. The signal was found to be reversible or quasi-reversible for $(1)^+$, $(2)^+$ and $(3)^+$, but not for $(4)^+$. This is not surprising as the stability of phenoxyl radicals substituted by electron-withdrawing groups is expected to be low.[6]

The electrochemical behaviour of the complexes has been studied by cyclic voltammetry in CH_3CN at 298 K (in the presence of 0.1 M TBAP as supporting electrolyte).

Table 3 Electronic properties of the copper(II) complexes

Complex	UV-vis [λ_{max}/nm (ε/M^{-1} cm^{-1})][a]
$(1H)^{2+}$	605 (85)
$(1)^+$	500 (880), 930 (130)
$(2H)^{2+}$	550 (240)[b]
$(2)^+$	535 (920), 930 (130)[b]
$(3H)^{2+}$	617 (115)
$(3)^+$	560 (1330), 660 (700) sh
$(4H)^{2+}$	630 (120)[c]
$(4)^+$	510 (910), 654 (260)[c]

[a] CH_3CN solutions, T = 298 K, sh = shoulder. [b] From ref. 6. [c] From ref. 7.

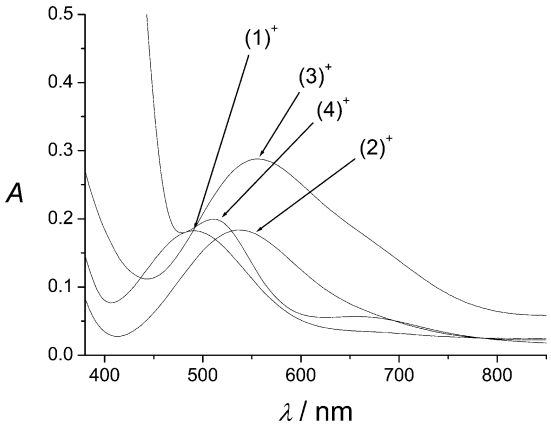

Fig. 3 UV-vis spectra of 0.2 mM CH_3CN solutions of $(1)^+$, $(2)^+$, $(3)^+$ and $(4)^+$. l = 1.0 cm, T = 298 K.

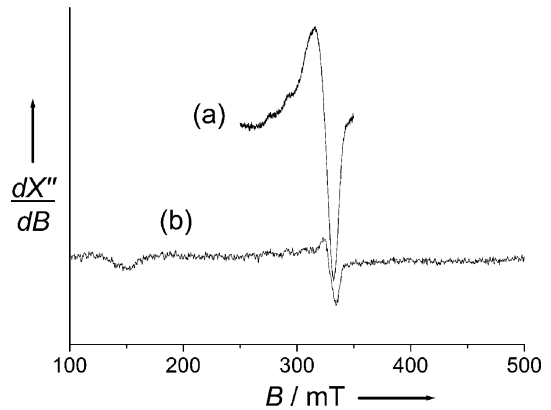

Fig. 4 X-Band EPR spectra of a 1 mM CH_3CN (+0.1 M TBAP) solution of (a) $(3)^+$ and (b) the electrogenerated $(3^{\bullet})^{2+}$. Microwave frequency 9.419 GHz, power 20 mW, modulation frequency 100 kHz, amplitude 0.197 mT, T = 100 K. The same scale is used along the y axis for both complexes. No signal was detected below 250 mT in the case of $(3)^+$.

The phenol complexes $(1H)^{2+}$, $(2H)^{2+}$, $(3H)^{2+}$ and $(4H)^{2+}$ exhibit, in the anodic region of potentials, an irreversible signal at values higher than 0.8 V *vs.* Fc/Fc^{+} attributed to the primary oxidation of the phenol moiety into a phenoxyl radical cation that decomposes irreversibly.[11]

Electrolysis of the phenolate complexes was performed at 233 K in CH_3CN under an inert atmosphere. Under these conditions only the one-electron oxidized species $(3^{\bullet})^{2+}$ could be generated (the other oxidized species were found to be too unstable). Its UV-vis spectrum is characterized by an intense transition at 425 nm (2940 M^{-1} cm^{-1}) and a lower intensity one at 545 nm (690 M^{-1} cm^{-1}) (Fig. 5). These bands are similar to those reported for the Cu^{II}-phenoxyl radical complex $[Cu^{II}(L^{OMe\bullet})(CH_3CN)]^{2+}$ (λ_{max} = 426 and 550 nm)[6] supporting the fact that $(3^{\bullet})^{2+}$ has a Cu^{II}-phenoxyl radical character. They are attributed to the π–π* transitions of the phenoxyl radical.[13] In addition, the 100 K EPR spectrum of $(3^{\bullet})^{2+}$ exhibits a signal at 150 mT corresponding to a forbidden $\Delta M_S = \pm 2$ transition as well as broader signals in the higher field region corresponding to $\Delta M_S = \pm 1$ transitions (Fig. 4). This shows that the copper(II) spin and the ligand radical spin are magnetically interacting in $(3^{\bullet})^{2+}$, and thus that the phenoxyl radical remains coordinated to the metal center. $(3^{\bullet})^{2+}$ was found to be relatively stable at 298 K as it decomposes in a first order process with k_{dec} = 0.013 min^{-1} ($t_{1/2}$ = 53 min). Its stability is somewhat lower than that of $[Cu(L^{OMe\bullet})(CH_3CN)]^{2+}$ (k_{dec} = 0.008 min^{-1}, $t_{1/2}$ = 87 min at 298 K)[6] showing that the N-donor ability of the ligand influences the stability of the Cu^{II}-phenoxyl radical species.[9]

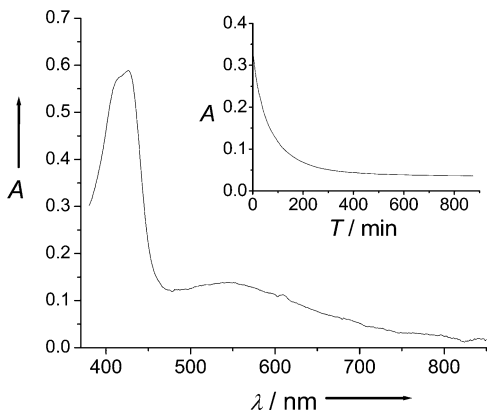

Fig. 5 UV-vis spectrum of a 0.2 mM CH_3CN solution (+0.1 M TBAP) of the electrogenerated $(3^{\bullet})^{2+}$. l = 1.0 cm, T = 233 K. The insert represents ΔA at 425 nm during decomposition of a 0.12 mM CH_3CN solution of the electrogenerated $(3^{\bullet})^{2+}$ at 298 K.

^{19}F NMR characterization of the copper complexes

The ^{19}F NMR spectra of $(1H)^{2+}$ and $(2H)^{2+}$ in CD_3CN–CH_3CN (1 : 4) are shown in Fig 6 and the chemical shifts are given in Table 4 (relative to C_6F_6 used as an external reference, $\delta_{C_6F_6}$ = –162.17 ppm *vs.* $CFCl_3$). $(1H)^{2+}$ and $(2H)^{2+}$ show single ^{19}F resonances at 99.6 ppm ($W_{1/2}$ = 16 Hz) and 41.9 ppm ($W_{1/2}$ = 23 Hz), respectively. For comparison, the free ligands HL^{CF3} and HL^{F} exhibit ^{19}F resonances at 100.6 and 34.0 ppm, respectively. The chemical shift is thus highly sensitive to the presence of metal and thus to complexation. The addition of NEt_3 to $(1H)^{2+}$ and $(2H)^{2+}$ induces both a downfield shift of the ^{19}F signal and

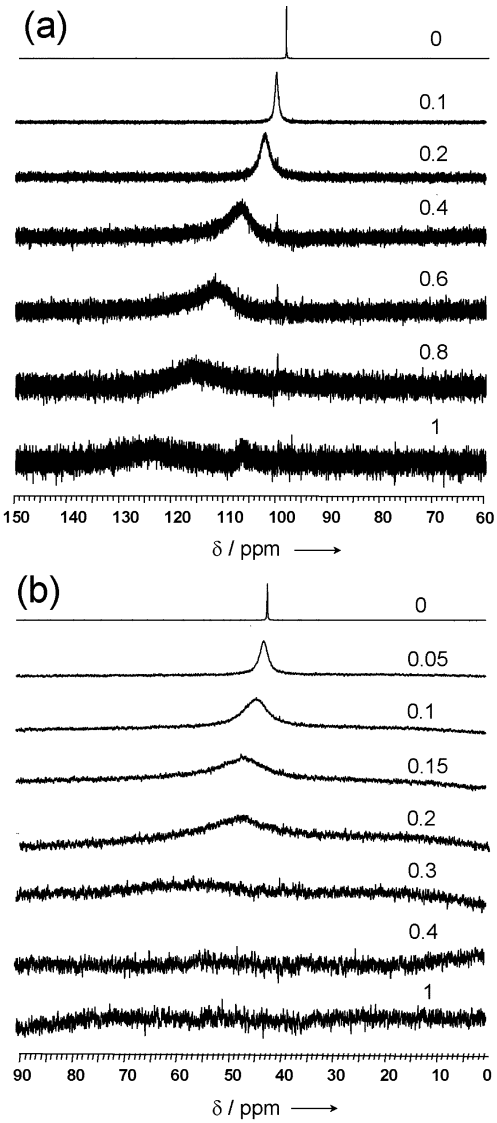

Fig. 6 Titration of 60 mM solution of (a) $(1H)^{+}$ and (b) $(2H)^{+}$ with NEt_3. NMR spectra recorded in (CD_3CN–CH_3CN) (1 : 4) at 298 K. The numbers correspond to the molar equivalents of copper added and the spectra are normalized.

Table 4 ^{19}F chemical shifts of the ligands and complexes

Species	δ/ppm[a]
HL^{CF3}	100.6
$(1H)^{2+}$	99.6 (16)
$(1)^{+}$	125 (3000)
HL^{F}	34.0
$(2H)^{2+}$	41.9 (23)
$(2)^{+}$	> 60 (n.d.)
HLq^{OMe}	46.2
$(3H)^{2+}$	53.6 (345)
$(3)^{+}$	49.0 (54)
HLq^{NO2}	46.0[b]
$(4H)^{2+}$	53.7 (250)[b]
$(4)^{+}$	49.0 (25)[b]

[a] δ given relative to C_6F_6 used as an external reference ($\delta_{C_6F_6}$ = –162.17 ppm *vs.* $CFCl_3$); $W_{1/2}$ (Hz) is indicated for the copper(II) complexes. [b] From ref. 7.

dramatic line broadening. This indicates that the Cu^{II}-phenol and Cu^{II}-phenolate complexes are in fast equilibrium at 298 K. For $(1H)^{2+}$, the ^{19}F resonance could be distinguished up to one molar equivalent of NEt_3 added. At this amount of NEt_3 added, the ^{19}F resonance is observed at $\delta_{C_6F_6} \approx 125$ ppm with a line width of *ca.* $W_{1/2} = 3000$ Hz. For $(2H)^{2+}$, the signal becomes barely observable at 0.3 molar equivalents of NEt_3 added, while it could not be observed above when 0.4 molar equivalents were added.

The sharper signal observed for $(1)^+$ compared to $(2)^+$ could be interpreted in terms of an increase in the fluorine–metal distance. The extra methylene group between the Cu and F atoms in $(1)^+$ makes the fluorine nucleus less sensitive to the copper(II) paramagnetism, resulting in a sharpening of the ^{19}F resonance. Spin rotation is also expected to contribute to the line width in a lesser amount.

The ^{19}F resonance was also found to be much sharper in the phenol than in the phenolate complexes. Deprotonation induces a contraction of the $Cu–O_{phenol}$ bond distance, and subsequent shortening of the fluorine–metal distance. In addition, a better electronic communication (through the π-system) exists between the copper and the fluorine atoms in the phenolate complexes. The fluorine atom thus becomes more sensitive to the copper paramagnetism in the phenolate complexes, inducing a dramatic broadening of the ^{19}F resonance.

Similar experiments have been undertaken on the phenol complexes $(3H)^{2+}$ and $(4H)^{2+}$. They exhibit single ^{19}F resonances at 53.6 ppm ($W_{1/2} = 345$ Hz) and 53.7 ppm ($W_{1/2} = 250$ Hz), respectively, higher values than those of the free ligands (46.0 and 46.2 ppm for HLq^{OMe} and HLq^{NO2}, respectively). One can note that the chemical shifts are poorly influenced by the nature of the phenol *para*-substituent, which is not surprising as there is no significant communication between the phenol and the quinoline ring.

Upon addition of NEt_3 to $(4H)^{2+}$, a broadening as well as an upfield shift of the ^{19}F signal is observed (Fig. 7). When exactly one molar equivalent of NEt_3 is added, the signal becomes much sharper ($\delta = 49.0$ ppm, $W_{1/2} = 25$ Hz), thus showing that the $(4H)^{2+}$ and $(4)^+$ species are in fast equilibrium at 298 K. A more complicated behaviour was observed upon addition of NEt_3 to $(3H)^{2+}$; a progressive disappearance and broadening of the $(3H)^{2+}$ signal is observed, concomitant with the appearance of a new broad signal originating from $(3)^+$ that increases in intensity. When exactly one molar equivalent of NEt_3 is added, the signal becomes much sharper, as observed for $(4)^+$. This behaviour is interpreted by the fact that 298 K roughly corresponds to the coalescence temperature in the $(3H)^{2+}$ and $(3)^+$ mixture.

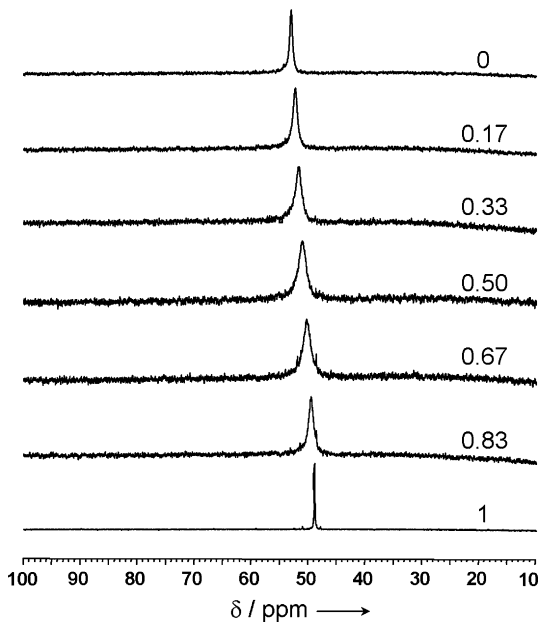

Fig. 7 Titration of $(4H)^{2+}$ (60 mM) with NEt_3; ^{19}F NMR spectra were recorded in ($CD_3CN–CH_3CN$) (1 : 4) at 293 K. The numbers correspond to the molar equivalents of base added and the intensities are normalized.

The phenolate complexes $(3)^+$ and $(4)^+$ thus exhibit a ^{19}F NMR signal that is significantly upfield shifted and much narrower than in the corresponding phenol species. This behaviour contrasts sharply with that of $(1)^+$ and $(2)^+$. In these latter cases, the signal observed for the phenolate complexes was found to be much broader and downfield shifted when compared to the phenol species.

As shown above, deprotonation induces a contraction of the $Cu–O_{phenol}$ bond. When the fluorine atom is incorporated on the phenol group, as in $(1H)^{2+}$ and $(2H)^{2+}$, the Cu–F distance varies concomitantly with the $Cu–O_{phenol}$ bond and the fluorine atom becomes more sensitive to the Cu^{2+} paramagnetism in the deprotonated complex.

In $(4H)^{2+}$, the X-ray structural analysis has shown that deprotonation is followed by a geometrical rearrangement; the phenolate shifts from the axial to the equatorial position, resulting in a shortening of the Cu–O bond. Simultaneously, the 6-fluoroquinoline moiety moves from the equatorial to the axial position. Axial bonds are known to be larger than equatorial ones; the enlargement of the $Cu–N_{quinoline}$, and consequently Cu–F, bond distances in $(4)^+$ makes the fluorine atom less sensitive to the Cu^{2+} paramagnetism in the presence of base. The ^{19}F NMR resonance is then sharper in $(4)^+$ compared to $(4H)^{2+}$.

Although the Cu^{II}-phenolate species $(3)^+$ could not be crystallized, the close similarity in the ^{19}F NMR spectra of $(3)^+$ and $(4)^+$ suggests an axial positioning of the quinoline group in the latter complex.[14]

Interconversion between $(4)^+$ and $(4H)^{2+}$

As shown above, protonation of $(4)^+$ into $(4H)^{2+}$ is accompanied by a molecular rearrangement. In $(4H)^{2+}$, the quinoline occupies the equatorial position, and the phenol weakly coordinates in the axial position, whereas in $(4)^+$, the quinoline moiety occupies an axial position, and the phenolate coordinates in an equatorial position. In order to get dynamic informations on the interconversion, we have recorded ^{19}F NMR spectra of equimolar mixtures of the Cu^{II}-phenol and Cu^{II}-phenolate complexes of HLq^{NO2} and HLq^{OMe} in ($CD_3CN–C_2H_5CN$) (1 : 4) as a function of the temperature.

For the $(4)^+$ + $(4H)^{2+}$ mixture, a broad resonance is observed down to 226 K, while at lower temperatures, the spectra consists of two distinct resonances at 49.0 and 53.7 ppm (Fig. 8). These signals are attributed to the $(4)^+$ and $(4H)^{2+}$ complexes that are in slow equilibrium at low temperature. At the coalescence temperature $T_C = 226$ K, according to eqn (1), a rate constant $k = 3000 \pm 100$ s^{-1} could be calculated for the equilibrium in eqn (2).[7,15] This rate constant is large, indicating that proton transfer and/or molecular re-arrangement (isomerization) is extremely rapid.

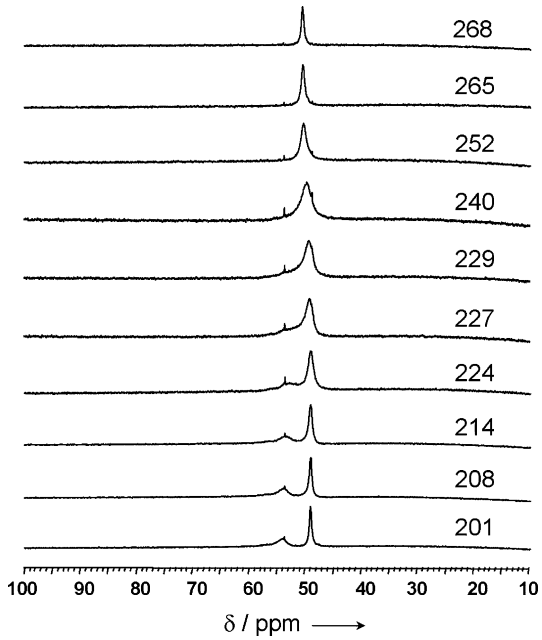

Fig. 8 Variable temperature ^{19}F NMR spectra of a (1 : 1) mixture of $(4)^+$ + $(4H)^{2+}$ (total = 2 mM) recorded in (CD_3CN–C_2H_5CN) (1 : 4); intensities are normalized, temperature (in K) is indicated at the right.

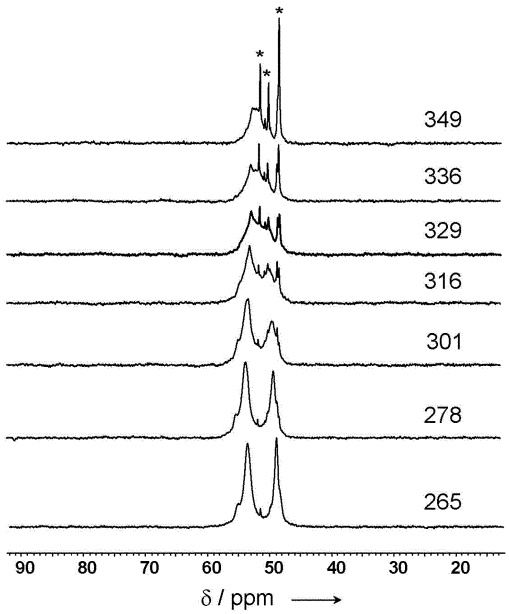

Fig. 9 Variable temperature ^{19}F NMR spectra of a (1 : 1) mixture of $(3)^+$ + $(3H)^{2+}$ (total = 20 mM) recorded in (CD_3CN–C_2H_5CN) (1 : 4); intensities are normalized, temperature (in K) indicated at the right. The stars denote unidentified diamagnetic impurities that appear upon an increase in the temperature (the temperature was lowered to 265 K and then increased up to 349 K during the experiment).

$$k = \frac{\pi \times \Delta\nu}{2^{1/2}} \quad (1)$$

$$(4)^+_A + (4H)^{2+}_B \rightleftharpoons (4H)^+_A + (4)^{2+}_B \quad (2)$$

(A and B represent two distinct complexes that interconvert.)

When the $(4)^+$ + $(4H)^{2+}$ mixture was replaced by the $(3)^+$ + $(3H)^{2+}$ mixture, a similar behaviour was observed but the coalescence temperature was found to be much higher. A significant decomposition is observed at high temperatures (sharp peaks denoted by stars on Fig. 9), thus precluding any accurate determination of T_C. Nevertheless, 330 K represents a reasonable approximation for the coalescence temperature. At this temperature, according to eqn (1), the rate constant for the equilibrium in eqn (2) was estimated to be 2900 ± 100 s^{-1}. Although it is found to be roughly similar to that obtained for the $(4)^+$ + $(4H)^{2+}$ mixture, the temperature at which it is calculated is much higher. This suggests that proton transfer and/or molecular re-arrangement is slower in the mixture $(3)^+$ + $(3H)^{2+}$, what may be ascribed to the increased basicity of a methoxyphenol compared to a nitrophenol.

The availability of crystal structures of both the $(4)^+$ and $(4H)^{2+}$ species makes $(4)^+$ the ideal candidate to study the acid-promoted isomerization by DFT calculations (Fig. 10 and 11).[16] The crystal structure of $(4)^+$ has been optimized and a proton has been added to the equatorial phenolate oxygen (structure A, Fig. 11). The system spontaneously evolves towards a complex involving an axial phenol in a multi-step process (Fig. 10). All the steps were shown to have favourable reaction energies and low activation barriers, in agreement with the high rate constant obtained experimentally.

The first step (limiting step) occurs with a low barrier of 2.4 kcal mol^{-1} and is found to be exothermic by 6.6 kcal mol^{-1}. It involves

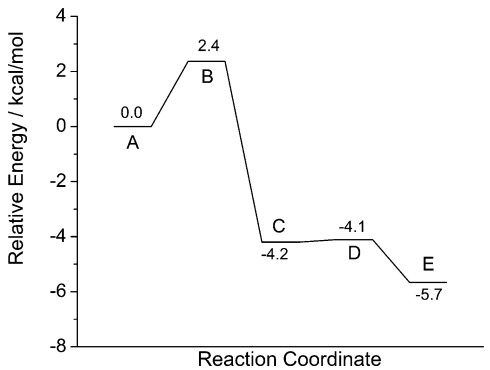

Fig. 10 Calculated B3LYP potential energy surface for the isomerization of $(4H)^{2+}$ at 0 K. The barriers are given by taking in account the zero point energy.

an increase in the Cu–O bond length and subsequent rearrangement of the three arms around the metal center. An optimized structure for the transition state (structure B) is shown in Fig. 11. It does not exhibit any π-stacking interactions between any of the aromatic rings. The τ value that represents the degree of distortion of a square pyramidal towards a trigonal bipyramidal geometry (0 corresponds to a perfect square pyramidal geometry, 1 a perfect trigonal bipyramidal geometry)[17] could be calculated to 0.71 for B, while it was only 0.09 for A. The geometry around the metal center is thus found to be best defined as trigonal bipyramidal in B, whereas it is essentially square planar in A. The Cu–O_{phenol} bond was found to be 2.27 Å, while one of the hydrogen atoms of the pyridine α-methylene group interacts with the phenol oxygen at a

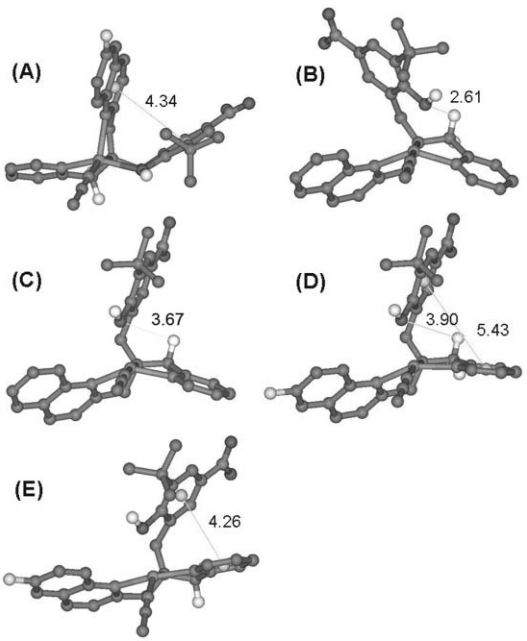

Fig. 11 B3LYP optimized structures for species A–E. The values indicated represent the distances between: (A) the centroids of the quinoline and phenol rings; (B–D) one hydrogen of the pyridine α-methylene group and the phenol oxygen; (D–E) the centroids of the pyridine and phenol rings.

O_{phenol}–$H_{methylene}$ distance of 2.61 Å. As a consequence, free rotation of the pyridine ring is severely perturbed.

The second step occurs with a very small barrier (less than 0.1 kcal mol^{-1}) if there is one. It involves stretching of the $O_{phenolate}$–$H_{methylene}$ bond that allows rotation of the pyridine ring. The transition state D exhibits $O_{phenolate}$–$H_{methylene}$ and Cu–O_{phenol} bond distances of 3.90 and 2.27 Å, respectively, while the metal ion adopts a geometry that is intermediate between square pyramidal and trigonal bipyramidal ($\tau = 0.31$). In the final species E (Fig. 11), the pyridine has slightly moved and the Cu–O_{phenol} bond distance stretches to 2.36 Å. This value is in perfect agreement with that of 2.363(3) Å obtained experimentally from the X-ray structural analysis. The geometry around the metal ion of E is best described as square pyramidal ($\tau = 0.15$) with the phenol ring located at the axial position. In addition, π-stacking interactions could be detected between the pyridine and the phenol ring, in agreement with the X-ray crystal structure of $(4H)^{2+}$. Although no perchlorate ion was included in our calculations, the ligand positioning in E is in very good agreement with that found in the crystal structure of $(4H)^{2+}$, confirming the validity of our method.

These results show that stretching of the Cu–O bond, π-stacking interactions and rotation of the pyridine are key steps in the isomerization process. It is interesting to compare these results with those obtained by Siegbahn *et al.* concerning the protonation step of Tyr_{495} of GO after substrate binding.[19] Prior to proton transfer (coordinated tyrosinate and bound alcohol) a minimum could be found in the potential surface energy only for models incorporating the peptidic link between Tyr_{495} and His_{496} (not for the models in which the amino acid residues are not linked). In this case, the barrier for the protonation of the tyrosinate residue was found to be small, lower than 3 kcal mol^{-1}, and the process exothermic by 3.2 kcal mol^{-1}. Tyr_{495} was found to dissociate upon protonation, as reflected by a Cu–O_{Tyr} bond distance of 2.86 Å, a value higher than that obtained in the X-ray crystal structure of GO (2.69 Å). In both the enzyme and our system the protonation process is thus found to be extremely rapid, even when isomerization occurs. In addition, these works highlight the important role of the link between one N-donor group and the phenol in order to maintain the O_{phenol} atom in the close vicinity of the copper ion.

Chemical generation and detection of a Cu^{II}-phenoxyl radical species by ^{19}F NMR

Upon addition of zero to one molar equivalent of copper(II) to $(3)^+$ at 238 K the violet CH_3CN solution turns dark green.[18] The absorbance at 560 nm progressively decreases, while new peaks appear at 425 and 550 nm. When exactly one molar equivalent is added, the spectrum was found to be identical to that of the electrogenerated $(3^{\bullet})^{2+}$ species. A Cu^{II}-phenoxyl radical species is thus formed according to eqn (3):[20]

$$(3)^+ + Cu^{II} \rightarrow (3^{\bullet})^{2+} + Cu^{I} \quad (3)$$

^{19}F NMR (Fig. 12) reveals that, upon addition of copper(II), a new resonance progressively increases in intensity at 53.7 ppm at the expense of the original signal at 49.0 ppm (corresponding to $(3)^+$). When one molar equivalent is added, the spectrum exhibits a single resonance at 53.7 ppm. This signal is attributed to the $(3^{\bullet})^{2+}$ radical complex that is in slow equilibrium with $(3)^+$ at 238 K. As the solution at the end of the titration may contain paramagnetic copper(II) impurities, further discussions concerning the difference in linewidth between $(3)^+$ and $(3^{\bullet})^{2+}$ is not possible.

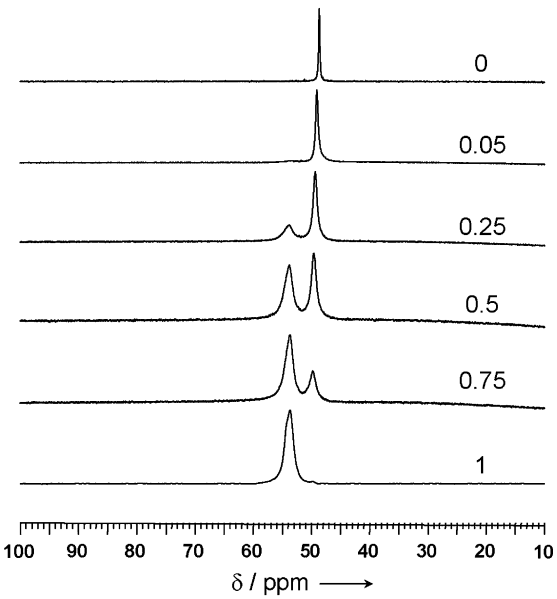

Fig. 12 Titration of $(3)^+$ (80 mM) with copper(II) perchlorate. NMR spectra recorded in (CD_3CN–CH_3CN) (1 : 4) at 238 K. The values correspond to the molar equivalents of copper added and the spectra are normalized.

A remarkable feature is that $(3)^+$ and $(3^{\bullet})^{2+}$ exhibit distinct chemical shifts although the Cu–$N_{quinoline}$ bond distances are not expected to be significantly different. In fact, $(3)^+$ and $(3^{\bullet})^{2+}$ exhibit

a different spin state, ($S = 1/2$) for the former and ($S = 1$) for the latter (see above). The fluorine atom is thus dramatically influenced by changes in the spin state of the complex, and not in the Cu–F distance. This makes ^{19}F NMR also an efficient probe for the phenolate oxidation state.

Conclusions

Key reactions that take place at the protein ligand during the GO catalytic cycle are proton transfer from the substrate to a tyrosinate residue and tyrosyl radical reduction. We have addressed here the basics concerning the use of ^{19}F NMR to monitor such phenomena in copper(II) complexes that model the enzyme active site.

The fluorine atom has been incorporated in N_3O tripodal ligands in two different ways: either at the phenol as a *para* substituent (HL^{CF3} and HL^{F}) or by replacing the pyridine group by a 6-fluoroquinoline (HLq^{OMe} and HLq^{NO2}). The copper(II) complexes of each ligand were characterized on their phenol and phenolate protonation states. Deprotonation induces contraction of the Cu–O_{phenol} bond and subsequent changes in copper–fluorine distance that could be easily vizualized by ^{19}F NMR. As the copper–fluorine distance decreases in $(1H)^{2+}$ and $(2H)^{2+}$, the ^{19}F resonance broadens (the fluorine atom is more sensitive to the metal paramagnetism). In contrast, it increases in $(3H)^{2+}$ and $(4H)^{2+}$ making the ^{19}F resonance sharper (the fluorine atom is less sensitive to the metal paramagnetism).

Protonation of $(4)^{+}$ was found to be accompanied by a rapid equatorial-to-axial isomerization of the phenol(ate) group. DFT calculations show that this process occurs with a low barrier, and that stretching of the Cu–O bond, π-stacking interactions and rotation of the pyridine are key steps in the isomerization process.

In order to extend this study, ^{19}F NMR spectroscopy has been used to detect phenoxyl radicals. For this purpose, the phenol *para*-substituent has to be strongly electron-donating. $(3)^{+}$ has been synthesized and successfully oxidized into a stable phenoxyl radical. We present herein the first ^{19}F NMR evidences for the formation of a phenoxyl radical.

The ^{19}F NMR technique is thus a very powerful tool that gives access to unprecedented information. Depending on the finality (probe for phenoxyl radical formation or highly sensitive probe for phenol deprotonation), the judicious labelling is either that realized on the N-donor or the O-donor.

One may envisage to use this elegant tool to study substrate binding on model compounds or the enzymes directly.[21] In addition, the ^{19}F signal of $(2H)^{+}$ was found to be extremely sensitive to NEt_3. This property could be potentially useful to detect traces of bases in organic media by ^{19}F NMR.

Experimental

General

All chemicals were of reagent grade and used without purification. NMR spectra were recorded on a Bruker AM 300 (^{1}H at 300 Mhz, ^{13}C at 75 Mhz and ^{19}F at 282 MHz). Chemical shifts are given relative to tetramethylsilane (TMS). C_6F_6 was used as an internal reference for ^{19}F NMR experiments ($\delta_{C_6F_6} = -162.17$ ppm *vs.* $CFCl_3$). Mass spectra were recorded on a Thermofinningen (EI/DCI) or a Nermag R 101 C (FAB+) apparatus.

UV-vis spectroscopy

UV-vis spectra were recorded on a Perkin Elmer Lambda 2 spectrophotometer equipped with a temperature controller unit set at 298 K. The quartz cell path length is 1.0 cm. Low temperature visible spectra were recorded on an UVIKON spectrophotometer equipped with a quartz Dewar (H.S. Martin Inc.) containing a 1.0 cm path length quartz cell. The rate constant for the self-decomposition of the radical species was obtained spectrophotometrically: the absorbance decay at 425 nm was fitted using the Biokine (Bio Logic Co., Claix, France) software.

EPR

X-Band EPR spectra were recorded on a BRUKER ESP 300E spectrometer equipped with a BRUKER nitrogen flow cryostat. The spectra were processed using the WINEPR software and simulated using the BRUKER SIMFONIA software.

Electrochemistry

The cyclic voltammograms of each compound (1 mM) in CH_3CN containing tetra-*n*-butyl ammonium perchlorate (TBAP) 0.1 M as the supporting electrolyte, were recorded on a CH Instrument 660 potentiostat at 298 K, under an Ar atmosphere, using a glassy carbon disc as the working electrode (3 mm diameter), a Pt wire as the secondary electrode, and an $Ag/AgNO_3$ 0.01 M as the reference electrode. The potential of the regular ferrocene/ferrocenium (Fc/Fc^{+}) used as an internal reference is +0.087 V under our experimental conditions. Electrolysis at a carbon felt electrode (10 × 10 × 10 mm) was performed at 233 K, under an Ar atmosphere, using a PAR 273 potentiostat.

Crystal structure analysis

For the structures of $(1H)^{2+}\cdot 2ClO_4^{-}$ and $(3H)^{2+}\cdot 2ClO_4^{-}$, collected reflections were corrected for Lorentz and polarization effects but not for absorption. The structure was solved by direct methods and refined using the TEXSAN software.[22] All non-hydrogen atoms were refined with anisotropic thermal parameters. Hydrogen atoms were generated in idealized positions, riding on the carrier atoms, with isotropic thermal parameters.

DFT calculations

All calculations were performed using the Gaussian 03 program[16] at the B3LYP level of theory and the LANL2DZ ECP basis set for Ni, C and H and LANL2DZdp ECP basis set for N and O.

Synthesis

2-*Tert*-butyl-6-{[(6-fluoro-quinolin-2-ylmethyl)-pyridin-2-ylmethyl-amino]-methyl}-4-methoxyphenol (HLq^{OMe}). 3-*Tert*-butyl-2-hydroxy-5-methoxybenzaldehyde (208 mg, 1 mmol), 6-fluoro-quinolin-ylmethyl)-pyridin-2-ylmethylamine (267 mg, 1 mmol) and 0.1 mL glacial acetic acid were dissolved in methanol (10 mL). Sodium cyanoborohydride (78 mg, 1.3 mmol) was added by small amounts, during 8 h. After 12 h stirring, the reaction mixture was neutralized by HCl (2 M), extracted with CH_2Cl_2 (2 × 50 mL), washed with saturated NaCl, dried over

Na_2SO_4 and evaporated. 2-*Tert*-butyl-6-{[(6-fluoro-quinolin-2-ylmethyl)-pyridin-2-ylmethyl-amino]-methyl}-4-methoxyphenol was purified by silica gel column chromatography with CH_2Cl_2–MeOH (30 : 1) as eluent. 2-*Tert*-butyl-6-{[(6-fluoro-quinolin-2-ylmethyl)-pyridin-2-ylmethyl-amino]-methyl}-4-methoxyphenol (275 mg, 60%) is obtained as a deep brown oil. ^{1}H NMR (300.12 MHz, $CDCl_3$, 298 K, TMS) δ/ppm: 1.50 (s, 9 H), 3.74 (s, 3 H), 3.84 (s, 2 H), 3.89 (s, 2 H), 4.03 (s, 2 H), 6.52 (d, ^4J(H,H) = 3.1 Hz), 6.82 (d, ^4J(H,H) = 3.1 Hz), 7.11 (dd, ^3J(H,H) = 7.4 Hz, 7.34–7.41 (m, 3 H), 7.47 (ddd, 1 H, ^3J(H,F) = 9.0 Hz, ^3J(H,H) = 8.5 Hz, ^4J(H,H) = 2.8 Hz), 7.56 (td, 1 H, ^3J(H,H) = 7.7 Hz, ^4J(H,H) = 1.8 Hz), 8.01 (d, ^3J(H,H) = 8.6 Hz), 8.19 (dd, 1 H, ^3J(H,H) = 9.2 Hz, ^4J(H,H) = 5.4 Hz), 8.52 (d, ^3J(H,H) = 4.9 Hz). ^{13}C NMR (75.465 MHz, $CDCl_3$, 298 K, TMS) δ/ppm: 30.1 (CH_3, *t*Bu), 35.4 (Cq), 53.8 (CH_2), 56.1 (OCH_3), 58.5 (CH_2), 59.8 (CH_2), 60.2 (CH_2), 110.9 (d, CH, ^2J(C,F) = 21.8 Hz), 112.9 (CH), 113.6 (CH), 120.0 (d, CH, ^2J(C,F) = 25.6 Hz), 122.0 (CH), 122.6 (CH), 123.6 (Cq), 123.9 (CH), 128.2 (d, Cq, ^3J(C,F) = 10.4 Hz), 131.7 (d, CH, ^3J(C,F) = 9.3 Hz), 136.3 (d, CH, ^4J(C,F) = 5.2 Hz), 137.0 (CH), 138.3 (Cq), 144.9 (Cq), 149.2 (CH), 150.7 (Cq), 151.0 (Cq), 158.4 (d, Cq, ^4J(C,F) = 2.8 Hz), 158.7 (Cq), 160.7 (d, Cq, ^1J(C,F) = 247.7 Hz). MS (DCI, NH_3 isobutane), *m*/*z*, 459 (M + H)$^+$. Anal. Calcd for $C_{38}H_{30}FN_3O_2$: C 66.07, H 6.08, N 8.04%. Found: C 66.08, H 6.10, N 8.41%.

2-*Tert*-butyl-4-trifluoromethylphenol. 4-Trifluoromethylphenol (1 g, 6.16 mmol) was dissolved in CH_3OH (1 mL) and *tert*-butanol (5 mL, 50 mmol) was added at room temperature. Sulfuric acid (92%, 5 mL) was then added dropwise at 273 K. After 12 h stirring, the reaction mixture was extracted with CH_2Cl_2 (2 × 50 mL), washed with saturated Na_2CO_3, dried over Na_2SO_4 and evaporated. 2-*Tert*-butyl-4-trifluoromethylphenol was purified by silica gel column chromatography with CH_2Cl_2–pentane (1 : 1) as eluent. 2-*Tert*-butyl-4-trifluoromethylphenol was obtained as a yellow oil with a yield of 80%. ^{1}H NMR (300.12 MHz, $CDCl_3$, 298 K, TMS) δ/ppm: 1.41 (s, 9H), 7.33 (dd, 1H, ^3J(H,H) = 8.3 Hz, ^4J(H,H) = 2.3 Hz), 7.51 (dd, 1H, ^4J(H,H) = 1.8 Hz). ^{13}C NMR (75.465 MHz, $CDCl_3$, 298 K, TMS) δ/ppm: 29.7 (CH_3, *t*Bu), 35.1 (Cq), 123.2 (q, Cq, ^2J(C,F) = 32.2 Hz), 124.8 (q, CH, ^3J(C,F) = 14.3 Hz), 124.9 (q, CH, ^3J(C,F) = 12.9 Hz), 125.0 (q, Cq, ^1J(C,F) = 271.3 Hz), 137.2 (Cq), 157.2 (Cq). MS (DCI, NH_3 isobutane), *m*/*z*, 218 (M + H)$^+$. Anal. Calcd for $C_{11}H_{13}F_3O$: C 60.54, H 6.00, F 26.12%. Found: C 59.79, H 6.04, F 26.04%.

2-*Tert*-butyl-6-{[bispyridin-2-ylmethyl-amino]-methyl}-4-trifluoromethylphenol (HL^{CF3}). 2-*Tert*-butyl-4-trifluoromethylphenol (1 g, 4.6 mmol), bis-methylpyridylamine (800 mg, 4.0 mmol) and paraformaldehyde (1 g, 30 mmol) were dissolved in ethanol (20 mL) and heated to reflux during 18 h. After evaporation, the oil was purified by silica gel column chromatography with CH_2Cl_2–CH_3OH (70 : 1) as eluent. 2[(Bis-pyridin-2-ylmethyl-amino)-methyl]-6-*tert*-butyl-4-trifluoromethylphenol was obtained as a colourless oil with a yield of 63%. ^{1}H NMR (300.12 MHz, $CDCl_3$, 298 K, TMS) δ/ppm: 1.47 (s, 9H), 3.85 (s, 2H), 3.89 (s, 4H), 7.13–7.18 (m, 3H), 7.29–7.31 (m, 2H), 7.41 (d, 1H, ^4J(H,F) = 1.9 Hz), 7.62 (td, 2H, ^3J(H,H) = 7.6 Hz, ^4J(H,H) = 1.8 Hz), 8.57 (d, 2H, ^3J(H,H) = 5.0 Hz, ^4J(H,H) = 1.8 Hz, ^4J(H,H) = 1.7 Hz). ^{13}C NMR (75.465 MHz, $CDCl_3$, 298 K, TMS) δ/ppm: 29.7 (CH_3, *t*Bu), 35.4 (Cq), 57.7 (CH_2), 59.5 (CH_2Py), 120.3 (Cq, ^2J(C,F) = 31.8 Hz), 122.7 (CH), 123.4 (Cq), 123.7 (CH), 123.8 (q, CH, ^3J(C,F) = 4.2 Hz), 125.2 (q, Cq, ^1J(C,F) = 271.3 Hz), 125.5 (q, CH, ^3J(C,F) = 3.8 Hz), 137.1 (CH), 137.6 (Cq), 149.4 (CH), 158.1 (Cq), 159.9 (Cq). MS (DCI, NH_3 isobutane), *m*/*z*, 428 (M + H)$^+$. Anal. Calcd for $C_{24}H_{26}F_3N_3O$: C 67.12, H 6.10, N 9.78, F 13.37%. Found: C 65.02, H 6.02, N 9.33, F 13.27%.

$(1H)^{2+}\cdot 2ClO_4^-$. To a CH_3CN solution (5 mL) of 2-*tert*-butyl-6-{[bispyridin-2-ylmethyl-amino]-methyl}-4-trifluoromethylphenol (190 mg, 0.443 mmol), a CH_3CN solution (1 mL) of $Cu(ClO_4)_2\cdot 6H_2O$ (164 mg, 0.528 mmol) was added dropwise. $(1H)^{2+}\cdot 2ClO_4^-$ was recrystallized by slow diffusion of Et_2O into the CH_3CN solution. Blue single crystals of $(1H)^{2+}\cdot 2ClO_4^-$ were collected by filtration (yield 65%). ESI MS, *m*/*z*: 491 (M – H – CH_3CN – $2ClO_4$)$^+$. Anal. Calcd for $C_{26}H_{29}Cl_2CuFN_4O_9$: C 42.60, H 3.99, N 7.64, Cu 8.67%. Found: C 42.78, H 4.05, N 7.61, Cu 8.80%. UV-vis in CH_3CN at 298 K (λ_{max}/nm (ε/M^{-1} cm^{-1})): 605 (85). EPR (9.41 GHz, CH_3CN, 100 K): $g_{xx} = g_{yy} = 2.054$, $g_{zz} = 2.240$, $A_{xx} = A_{yy} = 2$ mT, $A_{zz} = 18.2$ mT.

$(3H)^{2+}\cdot 2ClO_4^-$. 2-*Tert*-butyl-6-{[(6-fluoro-quinolin-2-ylmethyl)-pyridin-2-ylmethyl-amino]-methyl}-4-methoxyphenol (100 mg, 0.217 mmol) and $Cu(ClO_4)_2\cdot 6H_2O$ (80 mg, 0.217 mmol) were dissolved in CH_3CN (4 mL). $(3H)^{2+}\cdot 2ClO_4^-$ was recrystallized by slow diffusion of Et_2O into the CH_3CN solution. Blue single crystals of $(3H)^{2+}\cdot 2ClO_4^-$ were collected by filtration (100 mg, 50%). ESI MS, *m*/*z*: 521 (M – H – CH_3CN – $2ClO_4$)$^+$. Anal. Calcd for $C_{30}H_{33}Cl_2CuFN_4O_{10}$: C 47.22, H 4.36, N 7.34%. Found: C 47.17, H 4.28, N 7.39%. UV-vis in CH_3CN at 298 K (λ_{max} /nm (ε/M^{-1} cm^{-1})): 617 (115). EPR (9.41 GHz, CH_3CN, 100 K): $g_{xx} = g_{yy} = 2.063$, $g_{zz} = 2.253$, $A_{xx} = A_{yy} = 0.5$ mT, $A_{zz} = 17.6$ mT.

Notes and references

1 For reviews, see: J. W. Whittaker, in *Metal Ions in Biological Systems*, ed. H. Sigel and A. Sigel, Marcel Dekker, New York, 1994, vol. 30, pp. 315; C. D. Borman, C. G. Saysell, A. Sokolowski, M. B. Twitchett, C. Wright and A. G. Sykes, *Coord. Chem. Rev.*, 1999, **190–192**, 771; M. J. McPherson, M. R. Parsons, R. K. Spooner, C. M. Wilmot, in *Handbook for metalloproteins*, ed. A. Messerschmidt, R. Huber, T. Poulos and K. Wieghardt, John Wiley and Sons, 2001, vol. 2, pp. 1272; J. W. Whittaker, in *Advances in Protein Chemistry*, ed. F. M. Richards, D. S. Eisenberg and J. Kuriyan, Academic Press, Elsevier, 2002, vol. 60, pp. 1; J. W. Whittaker, *Chem. Rev.*, 2003, **103**, 2347; M. S. Rogers and D. M. Dooley, *Curr. Opin. Chem. Biol.*, 2003, **7**, 189; S. J. Firbank, M. Rogers, R. Hurtado-Guerrero, D. M. Dooley, M. A. Halcrow, S. E. V. Phillips, P. F. Knowles and M. J. McPherson, *Biochem. Soc. Trans.*, 2003, **31**, 506.

2 N. Ito, S. E. V. Philips, C. Stevens, Z. B. Ogel, M. J. McPherson, J. N. Keen, K. D. S. Yadav and P. F. Knowles, *Nature*, 1991, **350**, 87–90.

3 For recent articles, see: R. C. Pratt and T. D. P. Stack, *Inorg. Chem.*, 2005, **44**, 2367; P. Chaudhuri, K. Wieghardt, T. Weyhermüller, T. K. Paine, S. Mukherjee and C. Mukherjee, *Biol. Chem.*, 2005, **386**, 1023; A. Dos Anjos, A. J. Bortoluzzi, B. Szpoganicz, M. S. B. Caro, G. R. Friedermann, A. S. Mangrich and A. Neves, *Inorg. Chim. Acta*, 2005, **358**, 3106; F. Michel, S. Torelli, F. Thomas, C. Duboc, C. Philouze, C. Belle, S. Hamman, E. Saint-Aman and J.-L. Pierre, *Angew. Chem., Int. Ed.*, 2005, **44**, 438; A. Berkessel, M. Doucet, S. Bulat and K. Glaubitz, *Biol. Chem.*, 2005, **386**, 1035; M. A. Hossain, F. Thomas, S. Hamman, E. Saint-Aman, D. Boturyn, P. Dumy and J.-L. Pierre, *J. Pept. Sci.*, 2006, **12**, 612; E. Zueva, P. H. Walton and J. E. McGrady, *Dalton Trans.*, 2006, 159; L. Benisvy, E. Bill, A. J. Blake, D. Collison, E. S. Davies, C. D. Garner, G. McArdle, E. J. L. McInnes, J. McMaster, S. H. K. Ross and C. Wilson, *Dalton Trans.*, 2006, 258; C. Mukherjee, T. Weyhermüller, K. Wieghardt and P. Chaudhuri, *Dalton Trans.*, 2006, 2169; F. Michel, F. Thomas, S. Hamman, C. Philouze, E. Saint-Aman and J.-L. Pierre, *Eur. J. Inorg. Chem.*, 2006, 3684; E. Safaei, T. Weyhermüller, E. Bothe,

K. Wieghardt and P. Chaudhuri, *Eur. J. Inorg. Chem.*, 2007, 2334; O. Rotthaus, O. Jarjayes, F. Thomas, C. Philouze, E. Saint-Aman and J.-L. Pierre, *Dalton Trans.*, 2007, 889; A. Mukherjee, F. Lloret and R. Mukherjee, *Inorg. Chem.*, 2008, **47**, 4471; A. John, M. M. Shaikh and P. Ghosh, *Dalton Trans.*, 2008, 2815.

4 For reviews see: H.-J. Krüger, *Angew. Chem., Int. Ed.*, 1999, **38**, 627; S. Itoh, M. Taki and S. Fukuzumi, *Coord. Chem. Rev.*, 2000, **198**, 3; B. A. Jazdzewski and W. B. Tolman, *Coord. Chem. Rev.*, 2000, **200–202**, 633; P. Chaudhuri and K. Wieghardt, *Prog. Inorg. Chem.*, 2001, **50**, 151; W. Kaim, *Dalton Trans.*, 2003, 761; P. Chaudhuri, K. Wieghardt, T. Weyhermüller, T. K. Paine, S. Mukherjee and C. Mukherjee, *Biol. Chem.*, 2005, **386**, 1023; K. Ray, T. Petrnko, K. Wieghardt and F. Neese, *Dalton Trans.*, 2007, 1552; F. Thomas, *Eur. J. Inorg. Chem.*, 2007, 2379.

5 S. Itoh, M. Taki, S. Takayama, S. Nagatomo, T. Kitagawa, N. Sakurada, R. Arakawa and S. Fukuzumi, *Angew. Chem., Int. Ed.*, 1999, **38**, 2774; F. Thomas, G. Gellon, I. Gautier-Luneau, E. Saint-Aman and J.-L. Pierre, *Angew. Chem., Int. Ed.*, 2002, **41**, 3047; Y. Shimazaki, S. Huth, S. Hirota and O. Yamauchi, *Inorg. Chim. Acta*, 2002, **331**, 168; A. John, M. M. Shaikh and P. Ghosh, *Dalton Trans.*, 2008, 2815.

6 A. Philibert, F. Thomas, C. Philouze, S. Hamman, E. Saint-Aman and J.-L. Pierre, *Chem.–Eur. J.*, 2003, **9**, 3803.

7 F. Michel, S. Hamman, F. Thomas, C. Philouze, I. Gautier-Luneau and J. L. Pierre, *Chem. Commun.*, 2006, 4122.

8 R. Uma, R. Viswanathan, M. Palaniandavar and M. Lakshminarayanan, *J. Chem. Soc., Dalton Trans.*, 1994, 1219; H. Adams, N. A. Bailey, C. O. Rodriguez de Barbarin, D. E. Fenton and Q.-Y. He, *J. Chem. Soc., Dalton Trans.*, 1995, 2323; H. Adams, N. A. Bailey, I. K. Campbell, D. E. Fenton and Q.-Y. He, *J. Chem. Soc., Dalton Trans.*, 1996, 2233; M. Vaidyanathan, R. Viswanathan, M. Palaniandavar, T. Balasubramanian, P. Prabhaharan and T. P. Muthiah, *Inorg. Chem.*, 1998, **37**, 6418.

9 Y. Shimazaki, S. Huth, S. Hirota and O. Yamauchi, *Bull. Chem. Soc. Jpn.*, 2000, **73**, 1187; M. Taki, H. Hattori, T. Osako, S. Nagatomo, M. Shiro, T. Kitagawa and S. Itoh, *Inorg. Chim. Acta*, 2004, **357**, 3369.

10 S. Itoh, M. Taki, H. Kumei, S. Takayama, S. Nagatomo, T. Kitagawa, N. Sakurada, R. Arakawa and S. Fukuzumi, *Inorg. Chem.*, 2000, **39**, 3708; M. Taki, H. Kumei, S. Nagatomo, T. Kitagawa, S. Itoh and S. Fukuzumi, *Inorg. Chim. Acta*, 2000, **300–302**, 622.

11 F. Thomas, O. Jarjayes, C. Duboc, C. Philouze, E. Saint-Aman and J.-L. Pierre, *Dalton Trans.*, 2004, 2662.

12 J. Müller, T. Weyhermüller, E. Bill, P. Hildebrandt, L. Ould-Moussa, T. Glaser and K. Wieghardt, *Angew. Chem., Int. Ed.*, 1998, **37**, 616; E. Bill, J. Müller, T. Weyhermüller and K. Wieghardt, *Inorg. Chem.*, 1999, **38**, 5795; A. Sokolowski, H. Leutbecher, T. Weyhermüller, R. Schnepf, E. Bothe, E. Bill, P. Hildebrandt and K. Wieghardt, *JBIC, J. Biol. Inorg. Chem.*, 1997, **2**, 444.

13 H. M. Chang and H. H. Jaffe, *Chem. Phys. Lett.*, 1973, **23**, 146; H. M. Chang, H. H. Jaffe and C. A. Masmandis, *J. Phys. Chem.*, 1975, **79**, 1118; L. J. Johnston, N. Mathivanan, F. Negri, W. Siebrand and F. Zerbetto, *Can. J. Chem.*, 1993, **71**, 1655; J. Takahashi and T. Shida, *Bull. Chem. Soc. Jpn.*, 1994, **67**, 2038; J. Takahashi, T. Momose and T. Shida, *Bull. Chem. Soc. Jpn.*, 1994, **67**, 964; R. Liu, K. Morokuma, A. M. Mebel and M. C. Lin, *J. Phys. Chem.*, 1996, **100**, 9314; A. Hinchliffe, R. E. Steinbank and M. A. Ali, *Theor. Chim. Acta*, 1996, **5**, 95; J. G. Radziszewski, M. Gil, A. Gorski, J. Spanget-Larsen, J. Waluk and B. J. Mroz, *J. Chem. Phys.*, 2001, **115**, 9733.

14 If no rearrangement occurs, elongation of the Cu–N bond upon deprotonation should be less than 0.03 Å, which is too small to explain the observed differences in line widths.

15 H. Günther, *NMR spectroscopy*, John Wiley and Sons, New York, 2nd edn, 1992; $\Delta\nu$ corresponds to the chemical shift difference (in Hz) of the signals exchanging. The chemical shifts are independent of the temperature.

16 M. J. Frisch, G. W. Trucks, H. B. Schlegel, G. E. Scuseria, M. A. Robb, J. R. Cheeseman, J. A. Montgomery, Jr., T. Vreven, K. N. Kudin, J. C. Burant, J. M. Millam, S. S. Iyengar, J. Tomasi, V. Barone, B. Mennucci, M. Cossi, G. Scalmani, N. Rega, G. A. Petersson, H. Nakatsuji, M. Hada, M. Ehara, K. Toyota, R. Fukuda, J. Hasegawa, M. Ishida, T. Nakajima, Y. Honda, O. Kitao, H. Nakai, M. Klene, X. Li, J. E. Knox, H. P. Hratchian, J. B. Cross, V. Bakken, C. Adamo, J. Jaramillo, R. Gomperts, R. E. Stratmann, O. Yazyev, A. J. Austin, R. Cammi, C. Pomelli, J. Ochterski, P. Y. Ayala, K. Morokuma, G. A. Voth, P. Salvador, J. J. Dannenberg, V. G. Zakrzewski, S. Dapprich, A. D. Daniels, M. C. Strain, O. Farkas, D. K. Malick, A. D. Rabuck, K. Raghavachari, J. B. Foresman, J. V. Ortiz, Q. Cui, A. G. Baboul, S. Clifford, J. Cioslowski, B. B. Stefanov, G. Liu, A. Liashenko, P. Piskorz, I. Komaromi, R. L. Martin, D. J. Fox, T. Keith, M. A. Al-Laham, C. Y. Peng, A. Nanayakkara, M. Challacombe, P. M. W. Gill, B. G. Johnson, W. Chen, M. W. Wong, C. Gonzalez and J. A. Pople, *GAUSSIAN 03 (Revision C.02)*, Gaussian, Inc., Wallingford, CT, 2004.

17 A. W. Addison, T. N. Rao, J. Reedijk, J. van Rijn and G. C. Verschoor, *J. Chem. Soc., Dalton Trans.*, 1984, 1349.

18 The temperature was lowered to 238 K in order to prevent decomposition of the radical species.

19 F. Himo, L. A. Eriksson, F. Maseras and P. E. M. Siegbahn, *J. Am. Chem. Soc.*, 2000, **122**, 8031.

20 F. Michel, F. Thomas, S. Hamman, E. Saint-Aman, C. Bucher and J. L. Pierre, *Chem.–Eur. J.*, 2004, **10**, 4115.

21 P. K. Mykhailiuk, S. Afonin, G. V. Palamarchuk, O. V. Shishkin, A. S. Ulrich and I. Komarov, *Angew. Chem., Int. Ed.*, 2008, **47**, 5765.

22 *TEXSAN: Single Crystal Structure Analysis Software*, Molecular Structure Corporation, The Woodlands, TX, USA.

